



Pergamon

Available online at [www.sciencedirect.com](http://www.sciencedirect.com)

SCIENCE @ DIRECT®

OCEAN  
ENGINEERING

Ocean Engineering 30 (2003) 1353–1386

[www.elsevier.com/locate/oceaneng](http://www.elsevier.com/locate/oceaneng)

## Modeling of storm-induced coastal flooding for emergency management

K.F. Cheung <sup>a,\*</sup>, A.C. Phadke <sup>a, 1</sup>, Y. Wei <sup>a</sup>, R. Rojas <sup>a, 2</sup>, Y.J.-M. Douyere <sup>a</sup>, C.D. Martino <sup>a, 3</sup>, S.H. Houston <sup>b</sup>, P.L.-F. Liu <sup>c</sup>, P.J. Lynett <sup>c, 4</sup>, N. Dodd <sup>d</sup>, S. Liao <sup>e</sup>, E. Nakazaki <sup>f</sup>

<sup>a</sup> *Department of Ocean and Resources Engineering, University of Hawaii at Manoa, Honolulu, HI, USA*

<sup>b</sup> *Central Pacific Hurricane Center, National Weather Service, Honolulu, HI, USA*

<sup>c</sup> *School of Civil and Environmental Engineering, Cornell University, Ithaca, NY, USA*

<sup>d</sup> *School of Civil Engineering, University of Nottingham, Nottingham, UK*

<sup>e</sup> *School of Naval Architecture and Ocean Engineering, Shanghai Jiao Tong University, Shanghai, China*

<sup>f</sup> *Sea Engineering, Inc., Waimanalo, HI, USA*

Received 19 June 2002; accepted 18 September 2002

### Abstract

This paper describes a model package that simulates coastal flooding resulting from storm surge and waves generated by tropical cyclones. The package consists of four component models implemented at three levels of nested geographic regions, namely, ocean, coastal, and nearshore. The operation is automated through a preprocessor that prepares the computational grids and input atmospheric conditions and manages the data transfer between components. The third generation spectral wave model WAM and a nonlinear long-wave model calculate respectively the wave conditions and storm surge over the ocean region. The simulation results define the water levels and boundary conditions for the model SWAN to transform the storm waves in coastal regions. The storm surge and local tides define the water level in each nearshore region, where a Boussinesq model uses the wave spectra output from SWAN to simulate the surf-zone processes and runup along the coastline. The package is applied to hindcast the coastal flooding caused by Hurricanes Iwa and Iniki, which hit the Hawaiian Island of Kauai

\* Corresponding author. Tel.: +1-808-956-3485; fax: +1-808-956-3498.

E-mail address: [cheung@oe.soest.hawaii.edu](mailto:cheung@oe.soest.hawaii.edu) (K.F. Cheung).

<sup>1</sup> Presently at Sea Engineering, Inc., Houston, TX, USA

<sup>2</sup> Presently at INTEC Engineering Partnership, Ltd, Houston, TX, USA

<sup>3</sup> Presently at Pacific Missile Range Facility, Department of Defense, Kekaha, HI, USA

<sup>4</sup> Presently at Department of Civil Engineering, Texas A&M University, College Station, TX, USA

in 1982 and 1992, respectively. The model results indicate good agreement with the storm-water levels and overwash debris lines recorded during and after the events, demonstrating the capability of the model package as a forecast tool for emergency management.

© 2003 Elsevier Science Ltd. All rights reserved.

*Keywords:* Boussinesq model; Coastal flood hazards; Hurricanes; Inundation; Long-wave model; Spectral wave model; Tropical cyclones; Storm surge; Waves; Wave runup; Wave setup

---

## 1. Introduction

The Hawaiian and many other Pacific Islands are at risk of severe damage and life-threatening conditions from large swells and coastal flooding produced by tropical cyclones. The capability to forecast these events is critical to the early warning and evacuation procedures implemented by disaster management and relief agencies. Accurate prediction of storm-induced coastal flooding requires simultaneous simulation of several physical processes that include tropical cyclone winds and pressure, storm surge and waves, coastal wave transformation, surf-zone processes, and wave runup onto dry land. These processes, with different time and length scales, have been modeled separately with reasonable accuracy.

Tropical cyclones are one of the most difficult phenomena in the atmosphere to fully describe and predict. Mesoscale meteorological models, such as MM5, can provide three-dimensional wind and pressure fields resulting from multiple weather systems (Grell et al., 1994). The Geophysical Fluid Dynamic Laboratory (GFDL) model, on the other hand, provides three-dimensional simulation of a single tropical cyclone for forecast advisories (e.g. Kurihara et al., 1995, 1998). In the event of a hurricane, the Central Pacific Hurricane Center of the National Weather Service forecasts the track and intensity primarily based on operation experience with guidance from statistical and meteorological models. Once the track and intensity are predicted, simple parametric models can accurately describe the surface wind fields of tropical cyclones (e.g. Houston et al., 1999; and Phadke et al., 2003). Common parametric models include the modified Rankine model described by Hughes (1952), the SLOSH wind model proposed by Jelesnianski et al. (1992), and the Holland (1980) model. These physics-based and parametric models provide time-histories of surface wind and pressure fields to simulate the responses of the ocean.

Three-dimensional ocean models, such as POM, are available to simulate storm surge and currents together with other physical processes as tropical cyclones traverse the ocean surface (e.g. Kantha and Clayson, 1994). Depth-integrated long-wave models, on the other hand, provide a direct and efficient approach to describe storm surge and its coupling with astronomical tides (e.g. Westerink et al., 1992; and Bode and Hardy, 1997). Superimposed on these long ocean waves are surface gravity waves generated by wind shear stress. WAM is a third generation spectral model that simulates growth and propagation of surface waves in the open ocean based on wind energy input (WAMDI Group, 1988; and Zambresky, 1989). The spectral wave model SWAN calculates wave transformation and setup in the coastal region (Booij

et al., 1999; and Ris et al., 1999). Recent advances in Boussinesq-type models allow more accurate simulation of coastal wave transformation as well as surf-zone processes and runup onto dry land (e.g. Skotner and Apelt, 1999a, 1999b; Chen et al., 2000; and Lynett et al., 2002).

The processes that contribute to coastal flooding are coupled and need to be considered simultaneously to produce useful results for emergency management. Flather (2000) reviewed existing operational systems for real-time prediction of tides, surge, and waves in northwest Europe. Mastenbroek et al. (1993) incorporated the effect of wave-dependent drag on storm surge by using Janssen's theory (1991) to parameterize the surface roughness. Li and Zhang (1997) and Ozer et al. (2000) extended the approach to include two-way coupling between a spectral wave model and a storm surge model. The coupling of the spectral wave models WAM and SWAN is a standard approach to provide a complete description of wave generation and transformation from the open ocean to a coastal region (e.g. Wornom et al., 2001). Bao et al. (2000) coupled MM5, POM, and WAM to simulate the three-dimensional wind structures and ocean currents as well as the surface wave fields due to tropical cyclones. Phadke et al. (2003) applied parametric wind fields to simulate the surface circulation of a tropical cyclone to provide the atmospheric forcing in WAM and obtained accurate predictions of the wave heights near the core of the storm.

While the tools for forecasting occurrences such as tropical cyclone winds, surge, waves, and runup are readily available, a complete linkage between these events is less immediately evident. A forecast package for storm-induced coastal flooding, particularly for Hawaii and other Pacific islands characterized by steep nearshore bathymetry, requires a surf-zone processes and runup model to account for wave swashing. During Hurricane Iniki of 1992, the storm-water levels recorded by tide gauges, which included the storm surge, wave setup, and astronomical tides, were less than 2 m on the south shore of Kauai, but the floodwater reached the 9 m contour in the same area (Chiu et al., 1995). This paper describes the development and validation of an operational package at the University of Hawaii, in collaboration with the Pacific Disaster Center, Hawaii, to integrate the modeling of storm waves and surge generated by tropical cyclones as well as the subsequent coastal wave processes and runup onto dry land. The package is validated through hindcast studies of Hurricanes Iwa and Iniki, which hit the Hawaiian Island of Kauai in 1982 and 1992, respectively. These two radically different hurricanes provide a critical test of the predictive capability of the model package.

## 2. Model components

The model package assembled for the Pacific Disaster Center is customized to use a set of input parameters available through the National Weather Service Forecast Advisory products, which are issued every six hours during a tropical cyclone event. The operation specifications require the surge, waves, and inundation be predicted within the first 3 h of each advisory and that precludes the use of computationally intensive three-dimensional models. The need to rapidly deploy and apply the pack-

age to any location in the Pacific and Indian oceans rules out models that require pre-generated grids or labor-intensive grid editing and tuning. The assembled package has four major component models: a nonlinear long-wave model for storm surge, the spectral wave model WAM for wave generation and propagation in the open ocean, the model SWAN for coastal wave transformation, and a Boussinesq model to simulate surf-zone processes and runoff. This section provides brief descriptions of the four component models and the next section discusses their operation through a preprocessor program.

### 2.1. Storm surge

The depth-integrated, nonlinear long-wave equations can adequately describe the storm surge generated by tropical cyclones. Adapted from Mastenbroek et al. (1993), the governing equations written in terms of the longitude and latitude ( $\zeta$ ,  $\psi$ ) spherical coordinates include a continuity equation and two momentum equations in the  $\xi$  and  $\psi$  directions respectively,

$$\frac{\partial \zeta}{\partial t} + \frac{1}{R \cos \psi} \left[ \frac{\partial (Du)}{\partial \xi} + \frac{\partial (Dv \cos \psi)}{\partial \psi} \right] = 0 \quad (1)$$

$$\begin{aligned} \frac{\partial u}{\partial t} + \frac{u}{R \cos \psi} \frac{\partial u}{\partial \xi} + \frac{v}{R} \frac{\partial u}{\partial \psi} - \left( \frac{u \tan \psi}{R} + C_f \right) v = & - \frac{1}{R \cos \psi} \frac{\partial}{\partial \xi} \left( \frac{P_a}{\rho_w} + g \zeta \right) \\ & + \frac{1}{\rho_w D} \left( \tau_\xi - \tau_{b\xi} - \frac{1}{R \cos \psi} \frac{\partial S_{\xi\xi}}{\partial \xi} - \frac{1}{R} \frac{\partial S_{\xi\psi}}{\partial \psi} \right) \end{aligned} \quad (2)$$

$$\begin{aligned} \frac{\partial v}{\partial t} + \frac{u}{R \cos \psi} \frac{\partial v}{\partial \xi} + \frac{v}{R} \frac{\partial v}{\partial \psi} + \left( \frac{u \tan \psi}{R} + C_f \right) u = & - \frac{1}{R} \frac{\partial}{\partial \psi} \left( \frac{P_a}{\rho_w} + g \zeta \right) \\ & + \frac{1}{\rho_w D} \left( \tau_\psi - \tau_{b\psi} - \frac{1}{R \cos \psi} \frac{\partial S_{\psi\xi}}{\partial \xi} - \frac{1}{R} \frac{\partial S_{\psi\psi}}{\partial \psi} \right) \end{aligned} \quad (3)$$

where  $t$  denotes time,  $\zeta$  the water surface elevation,  $D = \zeta + h$  the instantaneous water depth with  $h$  being the local water depth, and  $(u, v)$  the depth-averaged velocity. The constants  $R$ ,  $\rho_w$ , and  $g$  denote respectively the earth radius, the water density, and the gravitational acceleration. The Coriolis effect is represented by the coefficient  $C_f$ , which is a function of the latitude  $\psi$ . The bottom shear stress  $(\tau_{b\xi}, \tau_{b\psi})$  is computed from an input Manning coefficient in terms of the depth-average flow velocity  $(u, v)$ . The system is forced externally by the atmospheric pressure  $P_a$ , the surface wind shear stress  $(\tau_\xi, \tau_\psi)$ , and the radiation stress  $S_{ij}$  ( $i, j = \xi, \psi$ ) from the storm waves.

The storm surge model SSM, used in the model package, is based on the governing equations (1) to (3) and their counterparts in the Cartesian coordinates as described by Mastenbroek et al. (1993). The solution is obtained using the numerical scheme developed by Liu et al. (1995) for tsunami modeling. The nonlinear long-wave equations are discretized using an explicit leap-frog finite-difference scheme with the

nonlinear convective terms evaluated by an up wind scheme. Up to four levels of nested spherical and rectangular grids of increasing resolution can be specified and the time-step size at each level of the nested grids must satisfy the Courant–Freidrich–Lewy (CFL) criterion. The nested grids are coupled and a complete cycle of information exchange occurs between two adjacent levels at each outer grid time step. The model can simulate absorbing and reflecting conditions for open boundaries and fixed coastlines respectively. If topographic data is provided, it can also simulate moving boundaries for the flooding and drying of coastal land resulting from the storm surge.

## 2.2. Waves in open ocean

The WAVE Model (WAM) is a third generation, spectral wave model. Komen et al. (1994) provided a detailed description of the theoretical background, numerical procedures, and application examples. The governing equation describes the energy balance for wave growth, propagation and dissipation based on wind energy input. The evolution of a two-dimensional wave spectrum  $F$  in time and space is defined by the transport equation

$$\frac{\partial F}{\partial t} + (\cos\xi\psi)^{-1} \frac{\partial}{\partial \xi}(\psi \cos \psi F) + \frac{\partial}{\partial \xi}(\dot{\xi} F) + \frac{\partial}{\partial \theta}(\dot{\theta} F) = S \quad (4)$$

where  $\theta$  is the wave direction,  $\dot{\xi}$  and  $\dot{\psi}$  represent the group velocity components in the respective coordinates,  $\dot{\theta}$  represents the rate of change of wave direction, and  $S$  includes energy input due to wind shear stress, dissipation due to white capping, and quartic energy exchange between wave components. A bottom friction term can be included in  $S$ , if wave shoaling and refraction are also considered.

The Deutsches Klimarechenzentrum at Hamburg, Germany supplied the WAM Cycle-4 source code. Günther et al. (1992) describes the input requirements and operations of WAM Cycle-4. The wave energy spectrum is discretized with constant directional and frequency resolution. The discrete frequencies are defined at equal increments between a user specified low-frequency cut-off and a fixed high-frequency cut-off at 1 Hz. The wave growth equation is solved using a second-order, central difference scheme with spherical or rectangular grids. The model allows two levels of coupled nested grids. The time step for the integration of the transport equation must meet the CFL criterion and be equal to or a multiple of the time interval of the source function integration. The model provides time series of the spectral wave parameters, wave-dependent surface wind shear stress ( $\tau_{\xi}$ ,  $\tau_{\psi}$ ), and wave radiation stress  $S_{ij}$  ( $i, j = \xi, \psi$ ) at specified locations or snapshots of the results over the entire region at specified times.

## 2.3. Coastal wave transformation

Simulating Waves Nearshore (SWAN) is a third-generation, spectral wave model that describes the evolution of two-dimensional wave energy spectra under specified

conditions of winds, currents, and bathymetry. Booij et al. (1999) and Ris et al. (1999) described the formulation and development of the wave model and its validation with field data. The basic equation used in SWAN is the action balance equation formulated by Hasselmann et al. (1973) and, in the Cartesian coordinates ( $x$ ,  $y$ ), is given by

$$\frac{\partial}{\partial t}N + \frac{\partial}{\partial x}c_x N + \frac{\partial}{\partial y}c_y N + \frac{\partial}{\partial \omega}c_\omega N + \frac{\partial}{\partial \theta}c_\theta N = \frac{S}{\omega} \quad (5)$$

where  $N$  is the wave action spectrum,  $\theta$  the wave direction, and  $\omega$  the intrinsic frequency. The first term on the left-hand side represents the local rate of change of action density in time. The second and third terms represent propagation of wave action with speeds  $c_x$  and  $c_y$  in the  $x$  and  $y$  directions, respectively. The fourth term represents shifting of the relative frequency due to variation in depth and current with the propagation speed  $c_\theta$  and the fifth term represents depth and current-induced refraction with the propagation speed  $c_\theta$ . The term  $S$  on the right-hand side represents the wind energy input, dissipation, and triad and quartic wave–wave interactions. Diffraction is not included in the version of the model used here.

The basic scientific philosophy of SWAN is similar to that of WAM, but its numerical schemes are quite different. The SWAN Cycle III User Manual by Holthuisen et al. (2000) provides a detailed account of the theoretical background, program structures, and implementation. The wave action density is discretized with constant directional and frequency resolution. Similar to WAM, the discrete frequencies are defined between a user-specified low-frequency cut-off and a fixed high-frequency cut-off at 1 Hz. The integration of the action balance equation is implemented with implicit finite difference schemes in a Cartesian or spherical coordinate system. These are first applied to the propagation of waves without the source term for generation, dissipation, and wave–wave interactions. The implementation of the source term is considered separately. A constant time step is used for the simultaneous integration of the propagation and the source terms. This is different from the time integration in WAM, where the time step for propagation can be different from the time step for the source term integration. The model allows the use of nested grids to successively provide high-resolution results at desired locations. In addition to output spectral wave parameters, SWAN also provides estimates of wave setup due to radiation stress.

#### 2.4. Surf-zone processes and runup

Lynett et al. (2002) described a Boussinesq-type equation model known as COUL-WAVE (Cornell University Long WAVE). The model allows for the evolution of fully nonlinear and weakly dispersive long and intermediate waves over variable bathymetry with provisions for wetting and drying of the coastal land. In contrast to the spectral wave model SWAN, this model provides a wave-by-wave simulation of the processes in the surf and swash zones, thereby providing an accurate description of the wave conditions along the coastline.

The depth-integrated governing equations of COULWAVE, in dimensionless form and Cartesian coordinates, are given as

$$\begin{aligned}
 \eta_t + \nabla \cdot [(h + \varepsilon\eta)\mathbf{u}_\alpha] - \mu^2 \nabla \cdot \left\{ (h + \varepsilon\eta) \left[ \frac{1}{6}(\varepsilon^2\eta^2 - \varepsilon\eta h + h^2) \right. \right. \\
 \left. \left. - \frac{1}{2}z_\alpha^2 \right] \nabla(\nabla \cdot \mathbf{u}_\alpha) + \left[ \frac{1}{2}(\varepsilon\eta - h) - z_\alpha \right] \nabla[\nabla \cdot (h\mathbf{u}_\alpha)] \right\} = O(\mu^4) \quad (6) \\
 \mathbf{u}_{\alpha t} + \varepsilon \mathbf{u}_\alpha \cdot \nabla \mathbf{u}_\alpha + \nabla \eta + \mu^2 \left\{ \frac{1}{2} z_\alpha^2 \nabla(\nabla \cdot \mathbf{u}_{\alpha t}) + z_\alpha \nabla[\nabla \cdot (h\mathbf{u}_{\alpha t})] \right\} \\
 + \varepsilon \mu^2 \left\{ [\nabla \cdot (h\mathbf{u}_\alpha)] \nabla[\nabla \cdot (h\mathbf{u}_\alpha)] - \nabla[\zeta(\nabla \cdot (h\mathbf{u}_{\alpha t}))] + (\mathbf{u}_\alpha \cdot \nabla z_\alpha) \nabla[\nabla \cdot (h\mathbf{u}_\alpha)] \right\} \\
 + \varepsilon \mu^2 \left\{ z_\alpha \nabla[\mathbf{u}_\alpha \cdot \nabla(\nabla \cdot (h\mathbf{u}_\alpha))] + z_\alpha (\mathbf{u}_\alpha \cdot \nabla z_\alpha) \nabla(\nabla \cdot \mathbf{u}_\alpha) + \frac{z_\alpha^2}{2} \nabla[\mathbf{u}_\alpha \cdot \nabla(\nabla \cdot \mathbf{u}_\alpha)] \right\} \quad (7) \\
 + \varepsilon^2 \mu^2 \nabla \left\{ -\frac{\eta^2}{2} \nabla \cdot \mathbf{u}_{\alpha t} - \eta \mathbf{u}_\alpha \cdot \nabla[\nabla \cdot (h\mathbf{u}_\alpha)] + \eta[\nabla \cdot (h\mathbf{u}_\alpha)] \nabla \cdot \mathbf{u}_\alpha \right\} \\
 + \varepsilon^3 \mu^2 \nabla \left\{ \frac{\eta^2}{2} [(\nabla \cdot \mathbf{u}_\alpha)^2 - \mathbf{u}_\alpha \cdot \nabla(\nabla \cdot \mathbf{u}_\alpha)] \right\} + \mathbf{R}_f - \mathbf{R}_b = O(\mu^4)
 \end{aligned}$$

where  $\eta$  denotes the free surface elevation, the subscript  $t$  indicates derivatives in time, and  $h$  is the local water depth. The reference velocity  $\mathbf{u}_\alpha = (u_\alpha, v_\alpha)$  is evaluated at  $z_\alpha = -0.531h$  based on the optimum agreement of the governing equations with the linear dispersion relation (Nwogu, 1993). The formulation is based on two dimensionless coefficients,  $\varepsilon = a/h$  and  $\mu = h/\lambda$ , where  $a$  is the wave amplitude and  $\lambda$  is the horizontal length scale. The coefficient  $\varepsilon$  indicates the importance of nonlinearity, while  $\mu$  is a second-order quantity representing frequency dispersion. The parameterizations  $\mathbf{R}_f$  and  $\mathbf{R}_b$  account for the effects of bottom friction and wave breaking, respectively. Bottom friction is described in the quadratic form (e.g. Chen et al., 2000), and wave breaking is approximated with the eddy viscosity technique, which introduces wave-slope dependent diffusive terms into the momentum equation (e.g. Zelt, 1991; and Kennedy et al., 2000).

The numerical solution utilizes a predictor-corrector time-integration scheme, accurate to the fourth order in terms of the time-step size. The finite difference scheme is accurate to the fourth order in terms of the spatial discretization, thereby minimizing numerical truncation errors in the spatial derivatives. The model simulates moving boundaries in the swash zone using a numerical technique similar to that implemented by Kowalik and Bang (1987) for the nonlinear shallow-water equations. The moving waterline is modeled by extrapolating the solution from the wet region onto the beach. This linear extrapolation locates the position of the waterline between wet and dry nodes, thereby allowing the real boundary to exist in-between grid points and improving the accuracy of the solution. The numerical results evaluated at the extrapolated waterline are used to update the solution for the next time

step. This moving-boundary technique is numerically stable and does not require any artificial dissipation mechanisms.

The computational domain is analogous to a rectangular laboratory wave basin with the modeled region located at one end and dissipative sponge layers placed along the other three walls. Along a pre-defined line within the computational domain, waves are generated using a source function approach. The free surface elevation along the line source is given by

$$\eta(x,y,t) = \sum_{i=1}^{M_\omega} \sum_{j=1}^{M_\theta} a_{ij} \sin[k_i(x \cos \theta_j + y \sin \theta_j) - \omega_i t + \phi_{ij}] \quad (8)$$

where  $a_{ij}$  is the discrete spectrum output from SWAN,  $k_i$  is the wave number,  $\phi_{ij}$  is a random phase shift, and  $M_\omega$  and  $M_\theta$  denotes the numbers of frequencies and directions bins, respectively. Based on the approach of Wei et al. (1999), the internal source generates the target waves through addition and subtraction of mass along the line source. Individual mass fluxes for the components are computed at each time step and are summed according to (8) to produce the prescribed surface elevation. The variation of the source function in time along the line simulates the excitation of a directional wave maker. Waves radiate out away from the line source in both directions. Those propagating toward the shoreline are considered in the study; dissipative sponge layers numerically absorb those propagating in other directions.

### 3. Model package

#### 3.1. System and operation

The four component models described in Section 2 are implemented at three levels of nested geographic regions, namely, ocean, coastal, and nearshore. Storm surge and waves are computed for the ocean and coastal regions, while surf-zone processes and runup are computed in the nearshore region. Fig. 1 illustrates the coupling of the four component models and their interface with the supporting utilities. The operation of the package is automated through a preprocessor program. The user specifies in the main input file:

- the modeled regions at the three levels,
- the file names and locations of user-supplied data files,
- the spatial and spectral resolution and time-step sizes,
- the best track of the tropical cyclone event, and
- the output requirements.

Each simulation covers a base-level ocean region and a number of nested coastal and nearshore regions. The types of external output include time series of wind, wave, current, and surface elevation data at specified locations or snapshots of the data over pre-defined output regions.

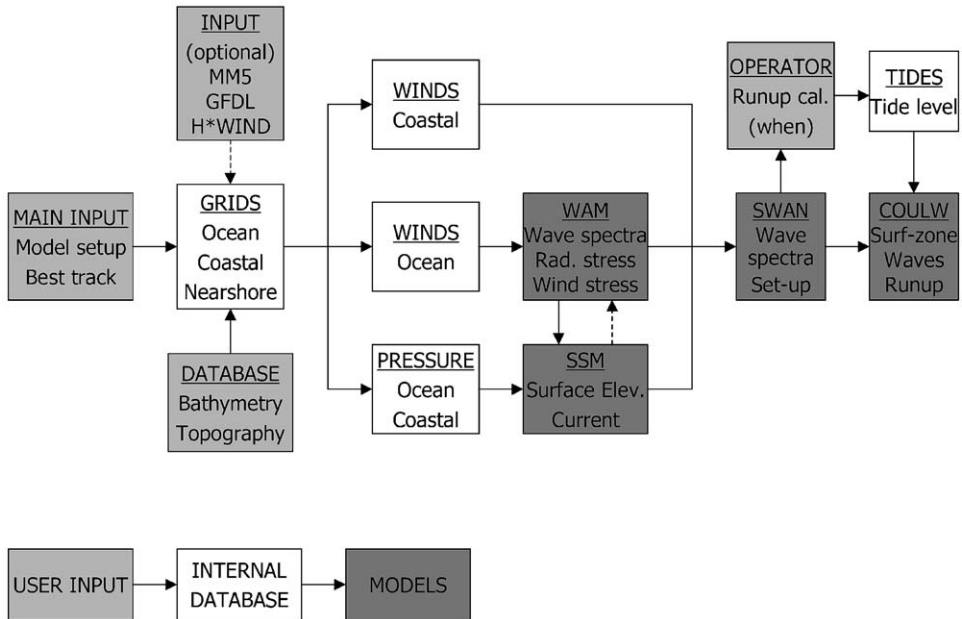


Fig. 1. Coupling scheme of model components and support utilities.

The boundaries of the ocean and coastal regions are defined along prescribed longitudes and latitudes. Each rectangular nearshore region is aligned with the local coastline and the orientation is defined by the bearing of the ocean-side boundary. The Generic Mapping Tool (GMT) developed by Wessel and Smith (1991) interpolates the user-supplied bathymetric and topographic data and generates the computational grids in the prescribed regions. The best track of a tropical cyclone includes the location, central pressure, and the radius of maximum winds as functions of time and provides the necessary information to generate the pressure and wind fields over the computational grids using parametric models. The Holland model defines the pressure distribution, while the modified Rankine vortex, the SLOSH wind, or the Holland model provides the hurricane wind fields with the forward-speed correction of Jelesnianski (1966) (see Phadke et al. (2003) for details). If available, GMT can interpolate the input wind fields over the computational grids using meteorological model output such as GFDL and MM5 or the observation-based H\*WIND data developed by the National Weather Service, Hurricane Research Division (Powell et al., 1996, 1998).

The base-level simulation covers the entire event of a tropical cyclone as it traverses the otherwise calm ocean region. The spectral wave model WAM and the storm surge model are coupled and run simultaneously to provide time-histories of the wave conditions, surface elevation, and currents over the entire region. WAM calculates the radiation stress and wave-dependent wind shear stress from the computed wave field for the input of the storm surge model. The current field computed

from the storm surge model in turn provides the background current for wave refraction calculation in WAM. However, the effect of the radiation stress from the surface waves on the depth-averaged current in the open ocean is insignificant. The depth-averaged current velocity, on the other hand, is often too small to have noticeable effects on the wave field in the open ocean. The coupling between the two models through the radiation stress and current is very weak as reported by Li and Zhang (1997) and is generally unnecessary for practical applications.

WAM outputs time-histories of wave spectra along the boundaries of pre-defined coastal regions, while the storm surge model provides the corresponding water levels within the regions. SWAN transforms the storm waves and calculates the wave setup in the coastal regions for the entire or a portion of the storm event. The bathymetry in each coastal region is modified continuously to account for the variation of the storm surge elevation as the tropical cyclone moves across the ocean region. SWAN outputs a time series of spectra at the offshore boundary of each nearshore region. The user evaluates the output water levels and wave conditions to determine the times when the inundation limits need to be evaluated in the nearshore regions. Since a nearshore region is small compared to the length scales of the astronomical tides and storm surge, the water level increases in the nearshore region are assumed to be uniform. The Boussinesq model provides a wave-by-wave description of a given sea state at the prescribed time and simulates the surf-zone processes and runup along the coastline of a nearshore region. The model automatically keeps track of all the wet computational grids to produce the inundation limit at the end of the simulation.

### 3.2. System structure

The model package runs on a PC-based Linux operating system and requires a FORTRAN 90 compiler and the programming language Octave. It can, however, be ported to other hardware/software platforms with relatively minimal effort. Tecplot and MATLAB are used for visualization of the model results. Fig. 2 illustrates the

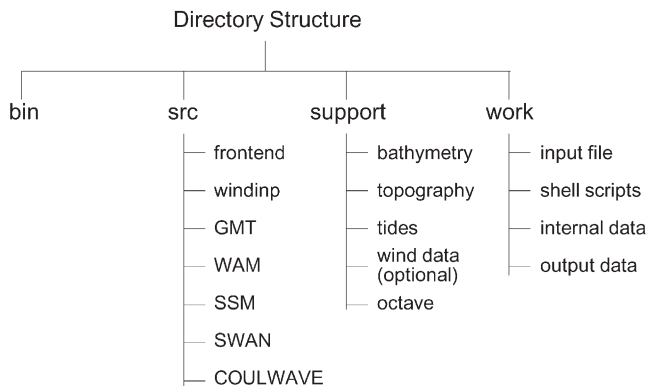


Fig. 2. Directory structure of model package.

directory structure and essential files. The *src* and *bin* directories respectively store the source code and executable files for the components of the package described in Section 3.1. User-supplied databases such as tidal constituents, bathymetry, topography, and optional wind input reside in the support directory. The work directory contains all the working files for a specific application that include the main input file, the shell script, the internally generated data files, and the output files. The preprocessor frontend in the *src* directory manages the data transfer and automates the simulation process with minimal user intervention.

The package creates standardized input and output files that can be read and interpreted by other component models and utility programs. The entire process is controlled by a separate shell program, which manages communications between components. GMT locates the bathymetric and topographic data in the support directory and generates the computational grids in the ocean, coastal, and nearshore regions. The computational grid data along with the wind and pressure fields generated by the program winding are stored in the work directory to provide the basic input to the four component models. The storm surge model and WAM are synchronized with data exchange at each time step. The output is automatically ported to the input files of the subsequent coastal SWAN simulation in the work directory. The output files from SWAN in turn are ported to the input files of the Boussinesq simulation in the nearshore regions. The package runs automatically until the end of the SWAN simulation, when the user examines the results and re-starts the execution to determine the inundation limits at a selected time.

The component models used in the package are continuously being refined to reflect the latest advancements in mathematical and numerical modeling techniques (e.g., Tolman, 2002; Tolman et al., 2002; and Rogers et al., 2002). Some of them are community models used around the world with frequent updates. One criterion of the development is to incorporate individual models with little or no change to the original code. The goal is to create a model package with a modular structure using the latest software. Should improvements be made to any of the programs used by the package, the updated version can replace the original and should fit seamlessly into the configuration of the package without disrupting the overall structure.

### 3.3. Validation

The model package is developed for emergency management and planning and therefore has been thoroughly tested before its implementation at the Pacific Disaster Center. Martino (2000); Rojas (2001); Douyere (2003), and Wong (2003) examined the package for various applications in the Pacific insular environment and verified the component models with field data and tested the result sensitivity. Phadke et al. (2003) provided additional validation of the parametric wind models with aircraft measured data during Hurricane Iniki 1992. Riegel and Vandamme (2002) applied the parametric wind models and WAM to simulate Hurricane Bonnie 1998 off the U.S. east coast and verified the results with buoy and aircraft measured wind and wave conditions described by Wright et al. (2001).

Rojas (2001) also tested the coupling schemes, model sensitivity, and operating

procedures and provided a user's manual for the model package. Sea Engineering Inc. (2002) performed the final testing and validation of the model package with water-level and inundation measurements obtained during and after Hurricanes Iwa and Iniki, which hit the Hawaiian islands of Kauai in 1982 and 1992, respectively. The package has been installed and tested at the Pacific Disaster Center for coastal flood hazards evaluation and prediction. The following sections summarize the analyses and findings of Rojas (2001) and Sea Engineering Inc. (2002) and the operation experience from the other studies using the model package.

## 4. Case studies

### 4.1. Storm events and data

There was an average of 3.2 tropical cyclones per year in the Central North Pacific basin during the period 1966–97 (Chu and Clark, 1999). Most of these storms passed well south or west of the Hawaiian Islands, or significantly weakened as they moved north toward Hawaii. Hurricane Iniki of 1992 and Iwa of 1982 are the most recent exceptions that approached Hawaii in hurricane strength and inflicted severe damage to the coastal communities. These two events, which brought extensive flooding to the Hawaiian Island of Kauai, are selected as the case studies to test the capability of the model package to hindcast the coastal flood conditions. Fig. 3 shows the paths of the two storms as their winds moved across the Hawaiian Islands. There were only four central pressure fixes during the entire event of Hurricane Iwa in contrast to the much better recorded Iniki. The locations of four National Data Buoy Center buoys in operation during Hurricane Iniki are also shown for reference.

Taken from the more detailed account by Storm Data (1992), the system that would later become Iniki was first declared to be a tropical depression 2690 km southwest of Baja California near 12°N 135°W on 6 September 1992. The storm was upgraded to hurricane strength, when it passed about 800 km south of Hawaii at 12:00 UTC 9 September. It later encountered a southwesterly flow from a weakening subtropical ridge, and began to turn northward at about 700 km south of Oahu. The eye of the storm reached Kauai at 01:20 UTC 12 September with a forward speed of 15 m/s and passed over the island in 40 minutes. Iniki was a Saffir-Simpson scale Category IV hurricane with a maximum sustained wind speed of 60 m/s and a minimum central pressure of 938 mbs. U.S. Air Force Reserves reconnaissance aircraft measurements are available for nearly 18 h from 10:00 UTC 11 September 1992 through the time of Iniki's landfall. Examination of the adjusted wind fields at the surface provides an average radius of maximum winds of 23 km, which is quite small for a storm of such intensity. Due to forward speed effects, the most severe wave conditions and coastal flooding occurred along the southeast coast of Kauai approximately 20 km east of the landfall.

Haraguchi (1983) provided a detailed account of Hurricane Iwa and its aftermath. The system that would later become Iwa was declared as a tropical storm 1500 km south of Hawaii near 9°N 166°W on 19 November 1982. The storm drifted north-

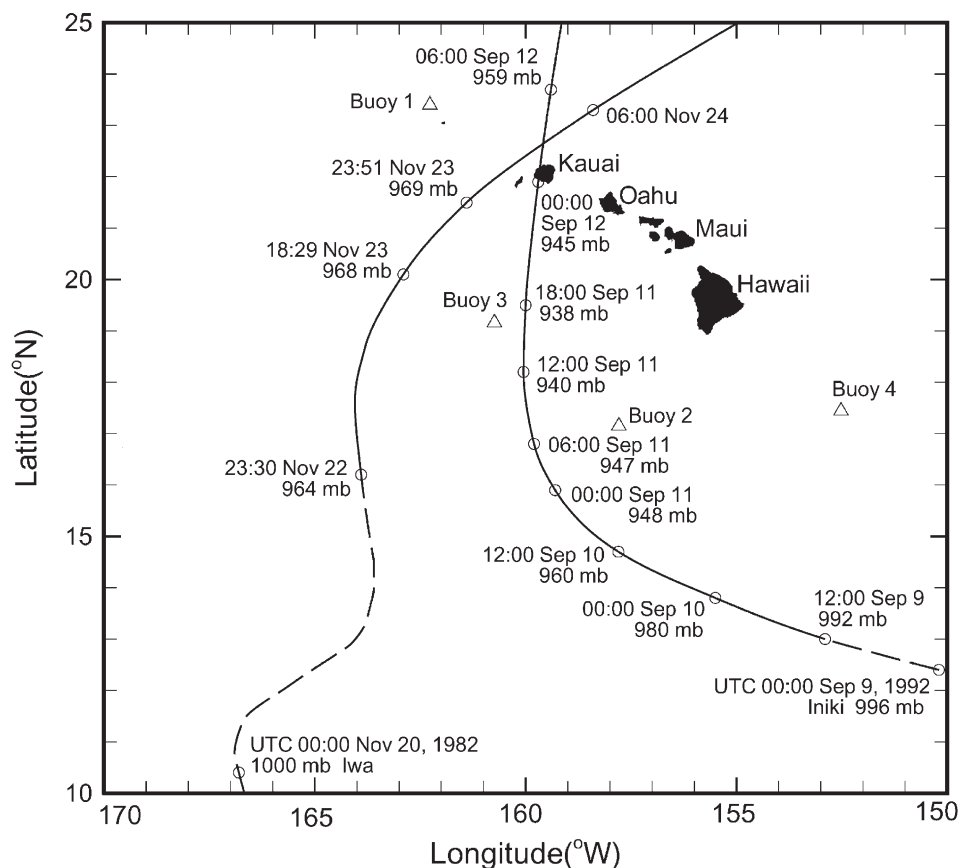


Fig. 3. Paths of Iwa 1982 and Iniki 1992. — —, tropical storm; —, hurricane.

ward, gradually gaining strength for the next 3 days, and was upgraded to hurricane status at 775 km southwest of Kauai near 16°N 164°W at 00:00 UTC 23 November. After moving north for 6 h to 19°N 164°W, Hurricane Iwa was caught in the southwesterly upper air flow and accelerated toward Kauai. Its center passed within 50 km northwest of Kauai with a maximum forward speed of 20 m/s at 03:00 UTC November 24. Aircraft measurements of the winds were unavailable at the time of the event. Sea Engineering Inc. and Bretschneider (1986) estimated the radius of maximum winds at 94 km based on the storm central pressure and the pressure measurements at Barbers Point, Honolulu, Lihue, and Barking Sands. Iwa was a Category I hurricane with a maximum sustained wind speed of 41 m/s and a minimum central pressure of 964 mb. It was less intense and more spread out in comparison to Iniki. Due to forward-speed effects, Iwa's most intense winds and waves occurred near the southeast coast of Kauai causing the most severe flooding. Because of the size of the storm, inundation also occurred on the southwest and south coasts of Oahu.

The best tracks of the Hurricane Iwa and Iniki supplied by National Weather Service along with the estimated radii of maximum winds are used in the parametric models to generate the input wind and pressure fields. Phadke et al. (2003) already validated the computed wind and wave fields of Iniki in the open ocean with aircraft and buoy measurements. The present paper focuses on the storm surge, coastal wave processes, and inundation predicted by the model package. The storm-water levels and inundation limits resulting from the two events were well recorded on the southern coast of Kauai near Poipu, where the most severe flooding occurred (e.g. Haraguchi 1983; Sea Engineering Inc. and Bretschneider, 1986; Sea Engineering Inc., 1993; and Fletcher et al., 1995). The two hurricanes have different characteristics and approach directions and provide distinctly different surge and wave conditions for the testing and validation of the model package for emergency management.

#### 4.2. Modeled regions and data

The case studies provide hindcast estimates of the storm-water levels and inundation limits along the south coast of Kauai resulting from Hurricanes Iniki 1992 and Iwa 1982. The storm tracks and the study location provide the necessary information to define the modeled regions and resolution. Fig. 4 shows the computational domains and bathymetry at the three levels of geographic regions. Although the model package allows multiple coastal and nearshore regions, only one of each is considered here. The same computational domains and resolution are used for both hurricane events. The modeled regions and resolution are selected to demonstrate and validate the model package, and the simulation therefore provides information that is more detailed and comprehensive than normally needed for emergency management.

Fig. 4a shows the ocean region, which extends from 10°N to 25°N and from 150°W to 170°W with a resolution of 0.1°. The computational domain covers a large ocean surface to the south of the study site to allow sufficient time and fetch for the development of the storm waves through the numerical simulation. The Earth-Topography-Two-Minute (ETOPO2) data from the National Geophysical Data Center provides the bathymetry over the region (Smith and Sandwell, 1997). The water depth around the Hawaiian Island chain is fairly uniform with an average of 4500 m. The resolution of 0.1° is reasonable for a small storm like Iniki, but is excessive for Iwa, which is four times larger. This resolution, however, is needed for proper transition to the more resolved coastal region around Kauai. The coastal region extends from 21.5°N to 22.5°N and from 159°W to 160°W as shown in Fig. 4b. It has a base resolution of 0.01° for the transition between the 0.1° ocean grid and the nested 0.001° coastal grids at Port Allen, Poipu, and Nawiliwili. Wave setup is computed at the nested grids to determine the storm-water levels. The wave spectra computed at the Poipu nested grid also provide input to the simulation in the embedded nearshore region as shown in Fig. 4c.

The SHOALS program of the U.S. Army Corps of Engineers provides detailed nearshore bathymetric and topographic data for Kauai. The nearshore bathymetric data was directly usable, but only a narrow strip of the topographic data along the

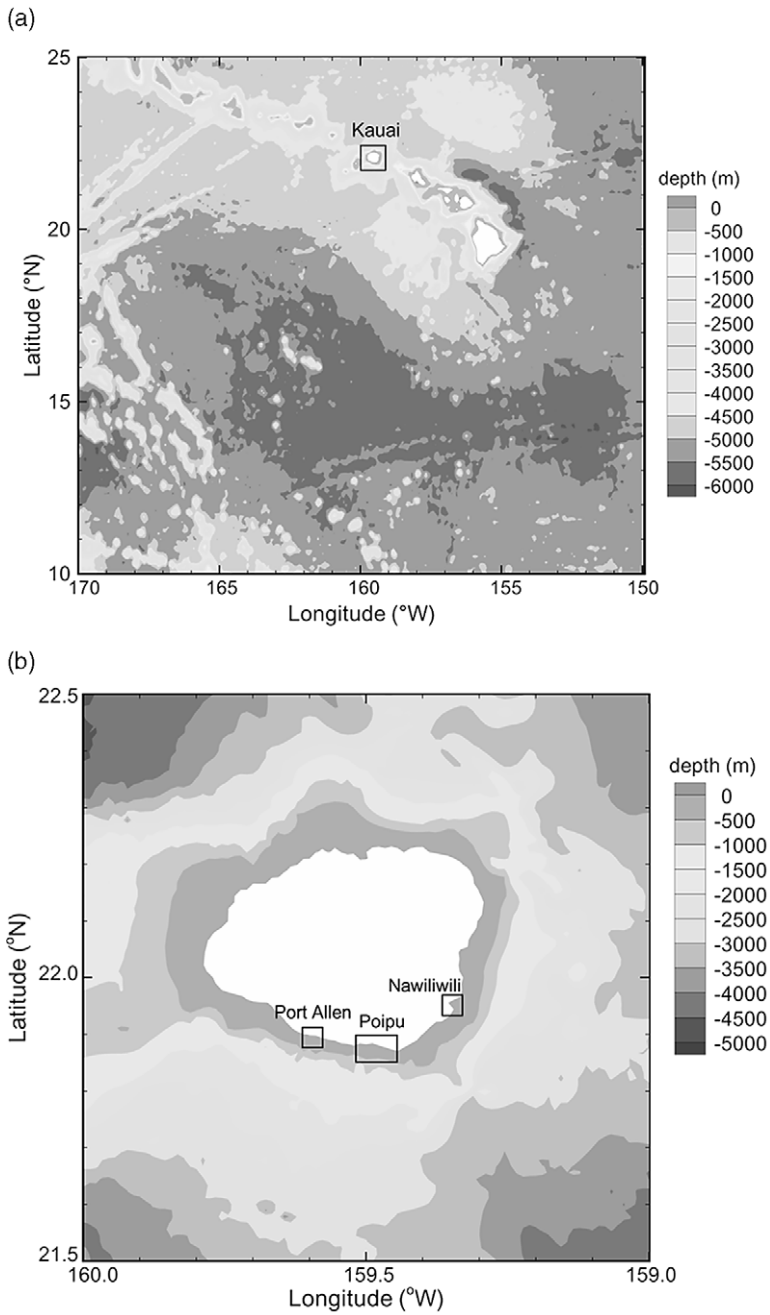
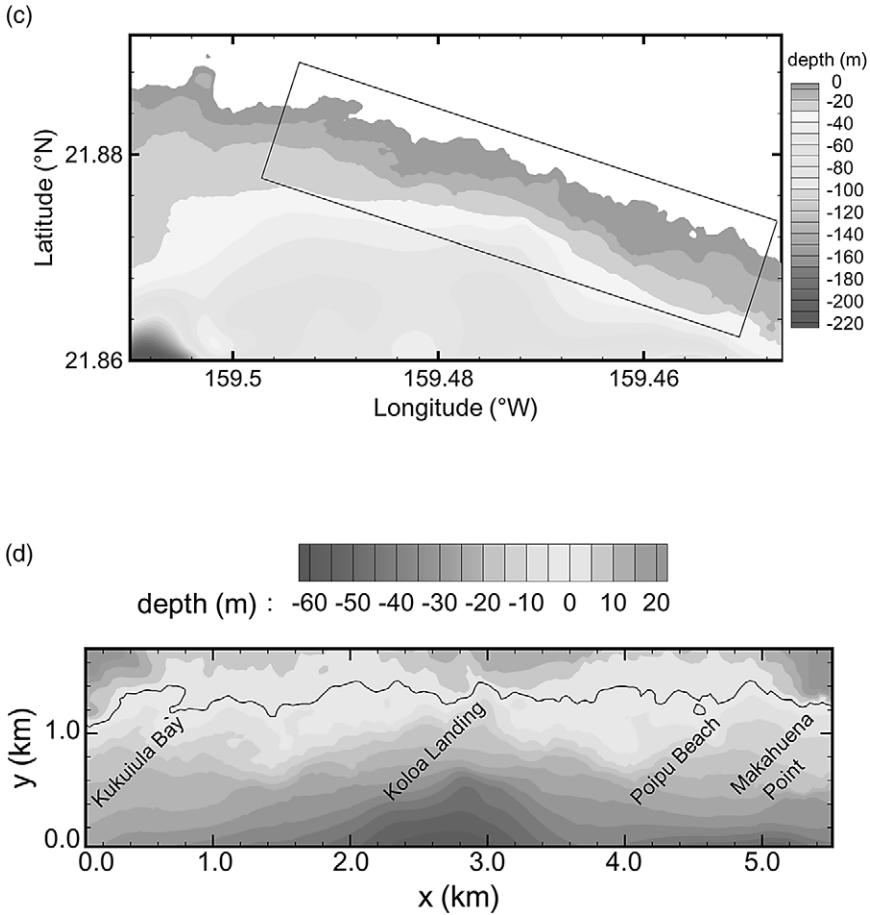


Fig. 4. Modeled regions at three geographic levels. (a) Ocean region. (b) Coastal region. (c) Nested coastal region at Poipu. (d) Nearshore region.

Fig. 4. *Continued*

shoreline is thus usable after the editing to remove irregularities. The topographic data inland is based on the topographic map of Kauai County Public Works Department, Area 3, Kalaheo-Lawai, Kolo-Poipu, produced in 1975. Fig. 4d shows the nearshore region defined within the nested coastal grid at Poipu. The nearshore region covers 5.2 km of shoreline with a resolution of 10 m. The nearshore slope is quite steep with no shallow reef flats along the shore. Kukuiula Bay is located at the west end of the computational domain. Its shoreline is rocky, with sea cliffs from 1.5 m to over 10 m high. East of Kukuiula Bay the backshore elevation is lower, with the 8-m contour generally being 300 m or more inland. The low-lying coastal region from Koloa Landing to Makahuena Point is extensively developed with hotels, condominiums, and dwellings. The 1-km long Poipu Beach consists of several beaches between rocky points along the coast. At Makahuena Point the shoreline is composed of rugged sea cliffs, rising steeply to the 15-m contour. The headlands at the west

and east ends of the computational domain act as a natural boundary condition in the model, restricting the lateral movement of the floodwater across the boundaries. A Manning coefficient of 0.03 is used to model the local terrain and vegetation over the coastal plain in this region (Bretschneider et al., 1986).

## 5. Results and discussion

### 5.1. Hurricane Iniki

The surge and wave conditions of Hurricane Iniki are simulated for a 3.5-day period starting 00:00 UTC 9 September, when the center of Iniki crossed into the ocean region at 150°W from the east. The initial condition corresponds to still water in the storm surge model and zero energy in the wave models. The surge and waves are generated by imposing the hurricane wind field. Phadke et al. (2003) compared the computed and measured wind and wave data and showed that the parametric wind models and WAM produce accurate results near the core of the storm. The modified Rankine wind model gives the best overall agreement and thus provides the input wind fields for the hindcast studies in this paper. Accurate simulation of the surge and waves requires proper settings of the runtime parameters.

The spectral wave simulations in the ocean and coast regions use a spectral resolution of 25 frequencies and 48 direction bins as recommended by Phadke et al. (2003). The lower frequency cut-off is defined at 0.0418 Hz corresponding to a period of 23.92 s. The time step sizes for WAM and SSM in the ocean region are 300 and 4 s, respectively. SWAN uses a time-step size of 300 s at both levels of nested grids in the coastal region, while COULWAVE uses a much smaller time step of 0.25 s to resolve the detailed wave field in the nearshore region.

The seabed slope around the Hawaiian Island chain is steep and the surrounding waters are relatively deep and uniform. The nonlinear coupling of storm surge and astronomical tides is not significant and is not needed for the simulation. Fig. 5a shows the computed storm surge of Hurricane Iniki at its maximum strength. The surge is primarily an axisymmetric dome of water responding to the barometric pressure drop around the storm center. The movement of the dome across the ocean surface generates long waves, which are refracted and diffracted around the Hawaiian Island chain. The change in the storm-surge level as Iniki makes landfall is minimal as shown in Fig. 5b. The computed maximum surge is 0.54 m corresponding closely to the storm central pressure of 947 mb at the time. The wave-radiation and wind-shear stresses as well as the bottom friction have little effect on the water-surface elevation due to the deep and steep bathymetry around the Hawaiian Islands. The calculated current speed is small and the effects of the currents on the storm waves are negligible.

The development of the storm waves is computed simultaneously with the storm surge. Fig. 6a shows the simulated wave field as Hurricane Iniki makes landfall and is moving rapidly north at a speed of 15 m/s. This forward velocity exceeds the group velocity of the waves and the storm outruns the circulation center of the wave

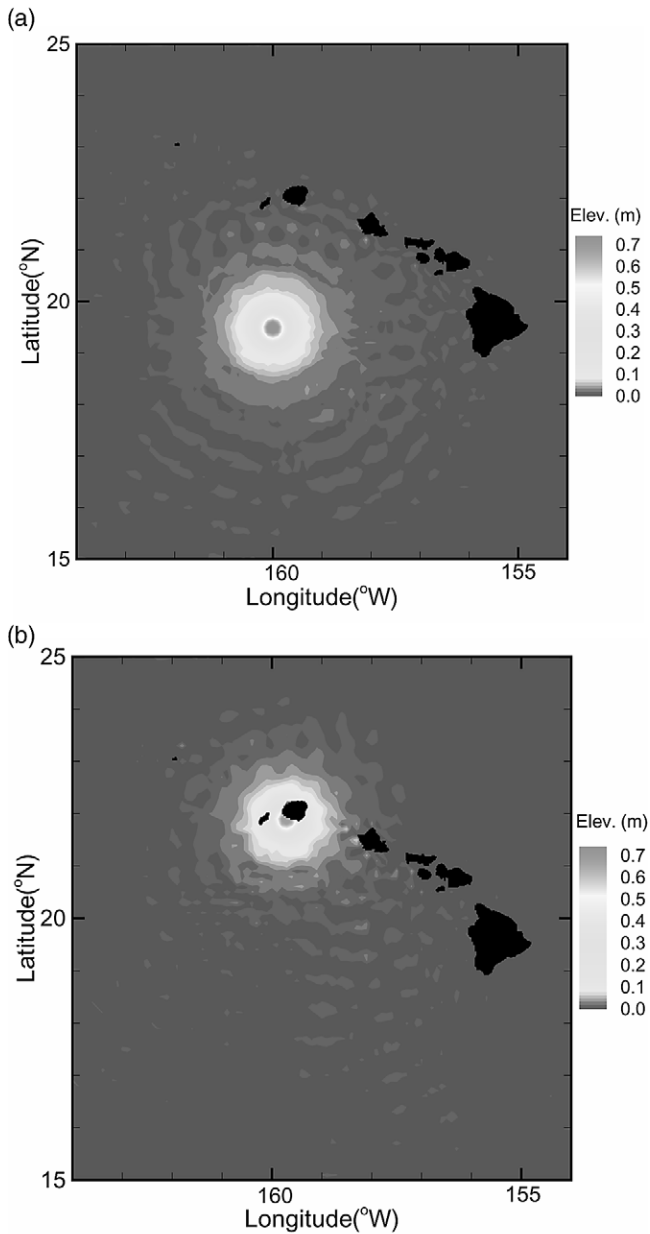


Fig. 5. Storm surge of Hurricane Iniki 1992. (a) Maximum pressure-drop at 18:00 UTC 11 September. (b) Landfall on Kauai at 01:20 UTC 12 September.

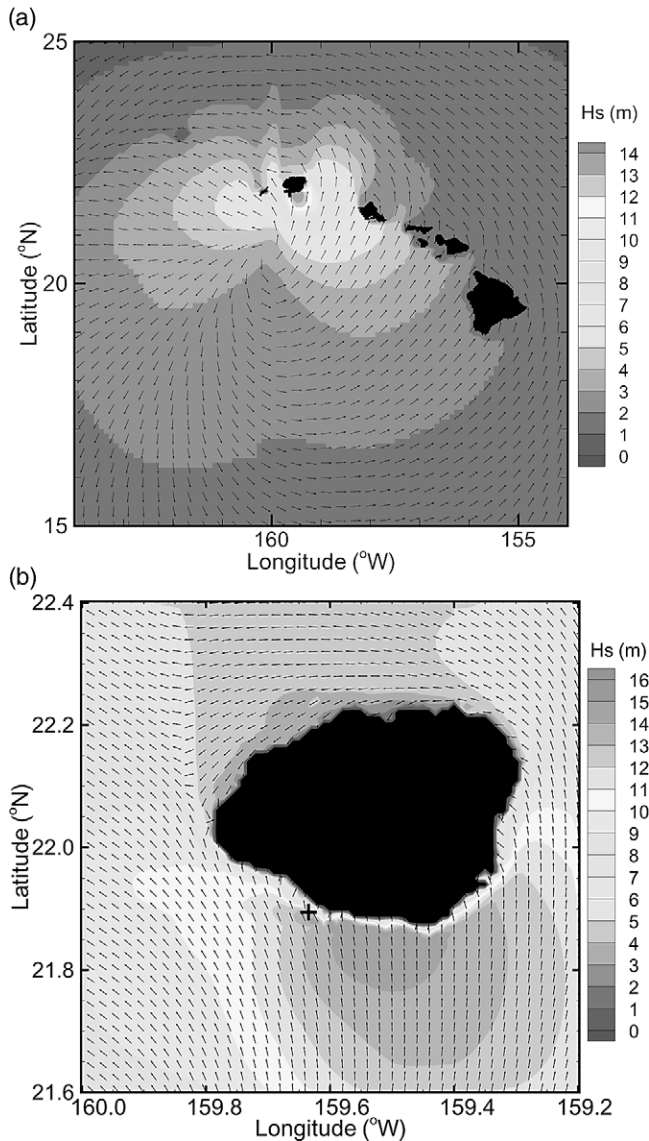


Fig. 6. Wave fields of Hurricane Iniki at landfall on Kauai. (a) Ocean region. (b) Coastal region. +, storm center.

field, producing a slight time lag between the peak wave and surge conditions. The model gives a maximum significant wave height of 13.3 m with a peak period of 11.8 s to the right of the storm center, just offshore of Poipu on the southeast coast of Kauai. The results provide the boundary conditions to simulate the wave trans-

formation in the coastal region around Kauai. The storm surge defines the time-dependent water level at the coastal region during the simulation. Fig. 6b shows the simulated waves wrapping around the island coast due to refraction. In contrast, the wave energy in the ocean region propagates along the channels and diffuses behind the individual islands.

The nested grids provide more resolved wave fields and estimates of wave set-up within the coastal region. Figs. 7a and 7b show respectively the wave field and setup off Poipu during the hurricane landfall. The offshore waves approach the coastline normally from the south and shoal to a maximum significant wave height of 14.9 m at 2.7 km from the shoreline. The spectral wave model does not fully account for the surf-zone processes and wave swashing, the computed wave conditions adjacent to the coastline, nevertheless provide a qualitative description of the event. The computed wave conditions away from the coastline, on the other hand, provide accurate input to the wave-by-wave simulation in the nearshore region. The computed wave setup is limited to a narrow region near the coastline and reaches a maximum level

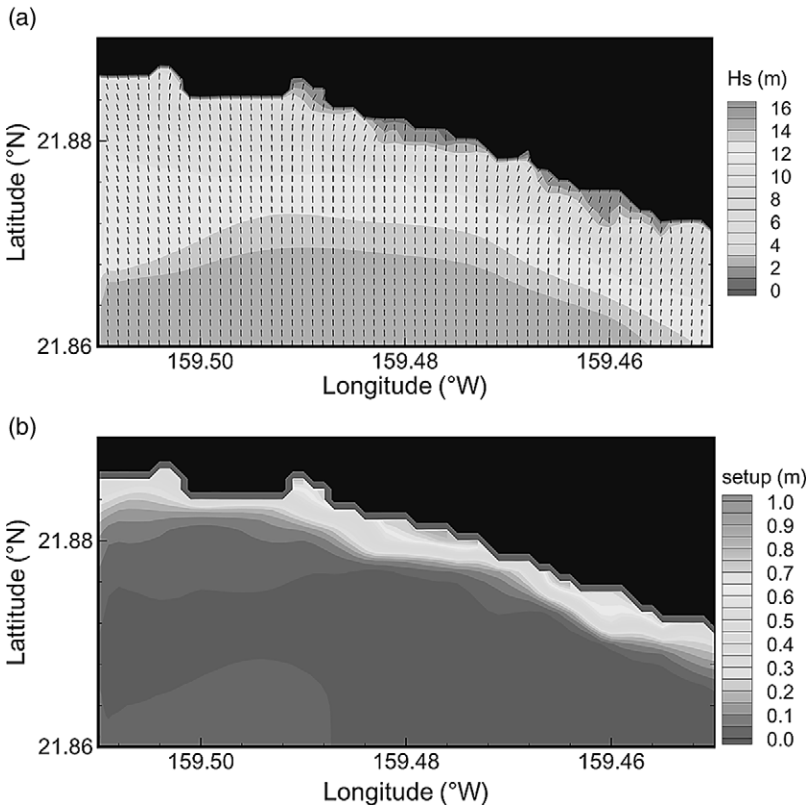


Fig. 7. Wave field and setup in the nested coastal region at Poipu during Hurricane Iniki at landfall. (a) Wave field. (b) Wave setup.

of 0.94 m at some locations. It is used along with the astronomical tides and storm surge to estimate the storm-water level.

Fig. 8 shows the time-histories of the computed storm-water levels and components at Port Allen and Nawiliwili Harbor located respectively on the south and southeast coasts of Kauai. The computed total water levels agree reasonably well with the tide-gauge records. Both tide gauges are located in harbor basins and recorded oscillations of the water levels during the peak of the event. The storm made landfall near Port Allen during neap-tide high water. The storm surge and wave set up superpose on the astronomical tides exacerbating the flood condition.

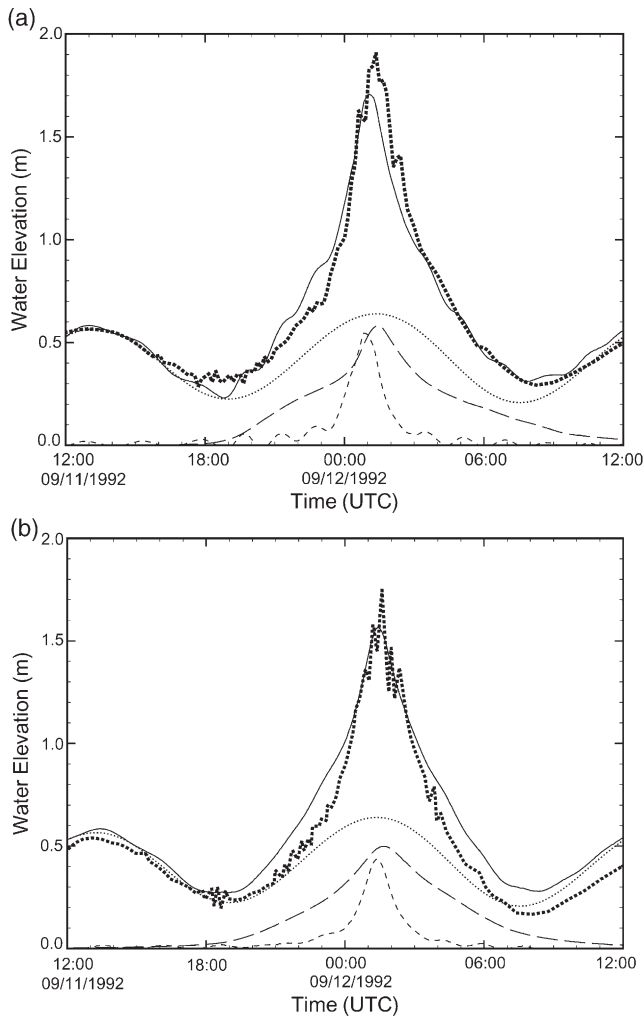


Fig. 8. Comparison of computed and measured water levels during Hurricane Iniki. (a) Port Allen. (b) Nawiliwili Harbor. ..... astronomical tides; - - - - storm surge; - - - wave setup; — storm water elevation; ■ recorded water elevation.

Because Iniki was a very small storm, the storm-surge level is smaller at Nawiliwili Harbor, located 25 km east of Port Allen. Wave set up is a gradual build-up of the water level along the coastline due to wave breaking and the associated surf-zone processes. It is not included in storm surge models commonly used in emergency management, but accounts for a significant portion of the total storm-water level in this case study.

Evaluation of the coastal wave conditions and storm-water levels determines that the maximum inundation is expected at landfall and identifies the wave spectrum and the astronomical tide and storm-surge levels for the nearshore region simulation. Sea Engineering, Inc. (2002) showed that a simulation time of 10 min is sufficient to produce statistically meaningful results from the wave-by-wave simulation in the nearshore region. Fig. 9 shows sample output of the wave fields at 6-s intervals after 8 min of simulation. The five snapshots cover approximately two wave cycles of simulation. Although not entirely visible in the figure, the results include coastal currents and wave setup due to breaking and other surf-zone processes. Due to the steep nearshore slope, the waves break very near to the shore and that results in a large swash zone. Flooding of the coastal plain is evident as the waterline does not fully recede over a wave cycle. Ponds in the low-lying backshore and islands of rocky areas are formed along the coastline.

The inundation limit is determined based on a 10-min simulation in the nearshore region. Fig. 10 compares the computed inundation limit and the overwash debris line recorded after the storm. The computed inundation limit generally follows the topography, while the debris line shows a more erratic pattern. The overall agreement between the computed and measured inundation is good. The largest discrepancies occur in the steep, narrow river valleys near Kukuila Bay and Koloa Landing, where the numerical model with a 10-m grid fails to resolve the flow in the 50-m wide valleys. The agreement will certainly be improved should a more resolved grid is used in the simulation. The storm-water level is less than 2 m at nearby Port Allen. Due to high surf, the floodwater typically reaches between the 4 and 6-m contours with a maximum between the 8 and 10-m contours at Koloa Landing. The results indicate that wave swashing is an important component in the total inundation and must be considered in the assessment of coastal flood hazards in Hawaii.

## 5.2. *Hurricane Iwa*

The surge and wave conditions of Hurricane Iwa are simulated for a 4.25-day period starting 00:00 UTC 20 November 1982, when the storm enters the computational domain at 10°N latitude from the south. The simulation uses the same time steps and spatial and spectral resolution as in the Iniki simulation. Fig. 11 shows plots of the computed storm surge when Iwa is at its maximum strength and at its closest approach to Kauai. The storm system is much larger than Iniki and the dome of water near the storm center has a more spread-out shape. The waves generated by the movement of the system have longer wavelengths and very small amplitudes, and exhibit less scattering around the Hawaiian Island chain in comparison to those of Iniki. The modeled surge reaches areas as far away as the south shore of Oahu.

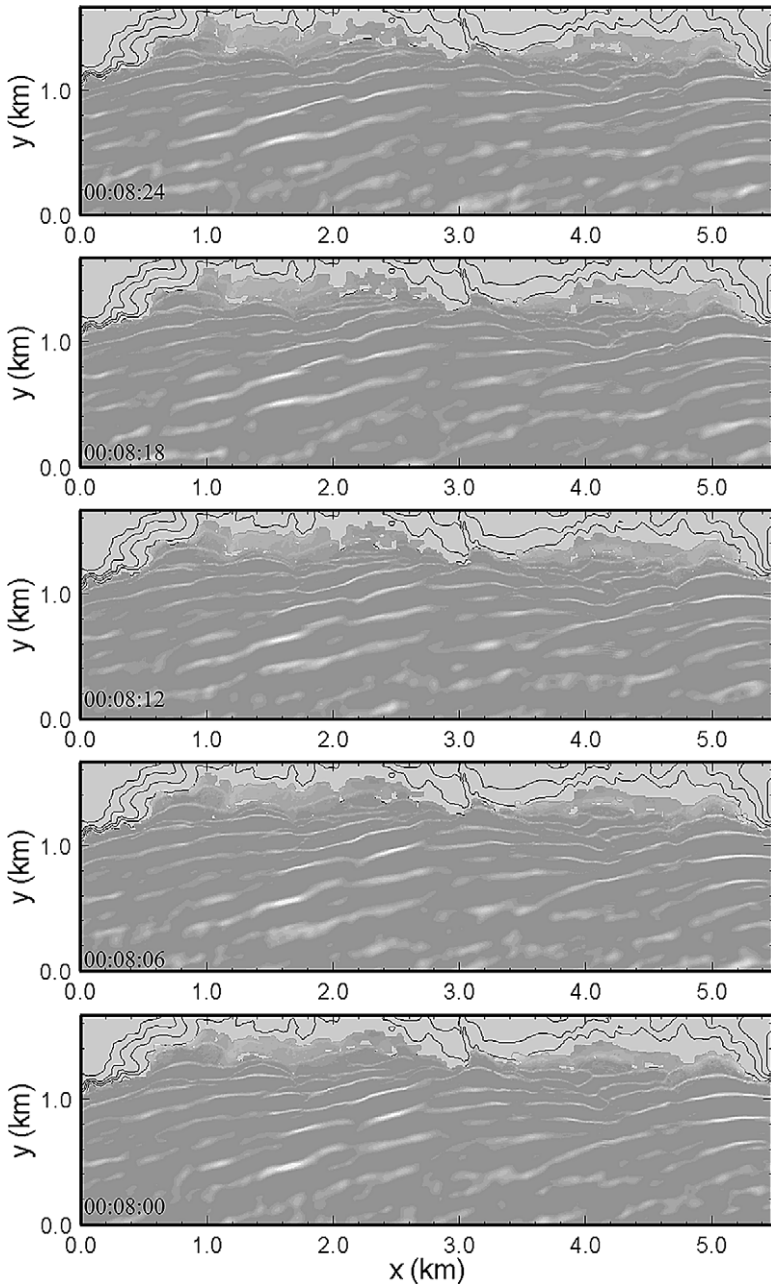


Fig. 9. Wave fields in nearshore region produced by Hurricane Iniki at landfall on Kauai.

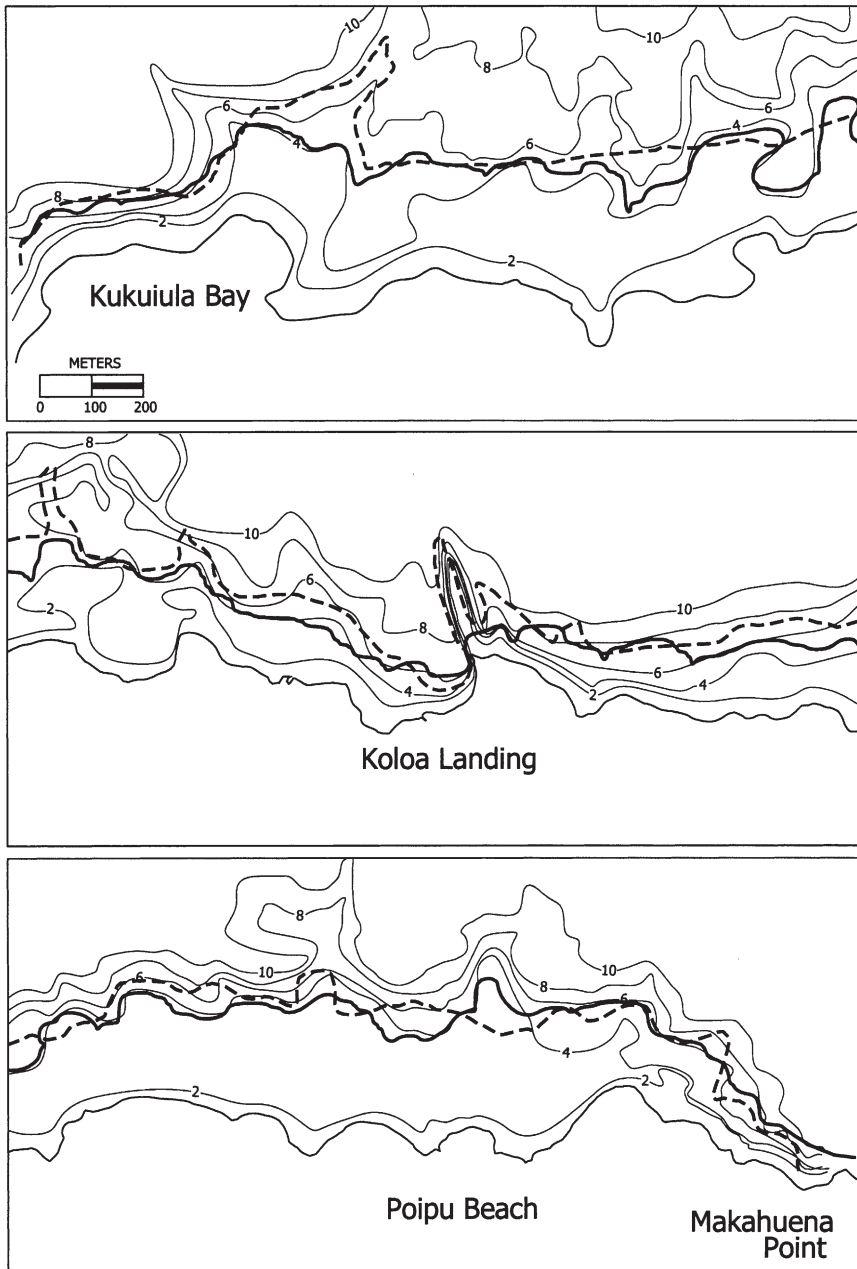


Fig. 10. Comparison of computed and measured inundation at Poipu, Kauai for Hurricane Iniki 1992. -----, overwash debris line; —, computed inundation limit.

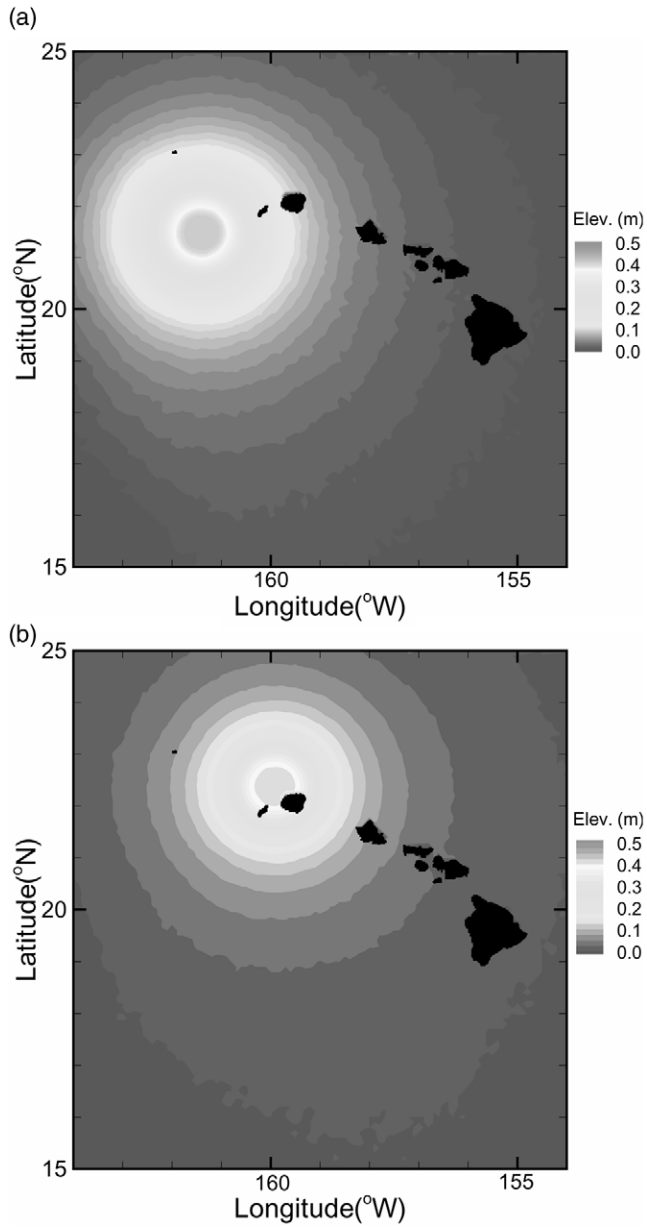


Fig. 11. Storm surge of Hurricane Iwa 1982. (a) Maximum pressure-drop at 00:00 UTC 24 November. (b) Closest approach to Kauai at 03:00 UTC 24 November.

This corroborates the unusual rise of water levels at tide gauges around Oahu during the storm (Haraguchi, 1983).

Fig. 12 shows the wave fields in the ocean and coastal regions when Iwa was nearest to Kauai. The model indicates a maximum significant wave height of 16.6 m with a peak period of 14.0 s at the channel between Kauai and Oahu. As the

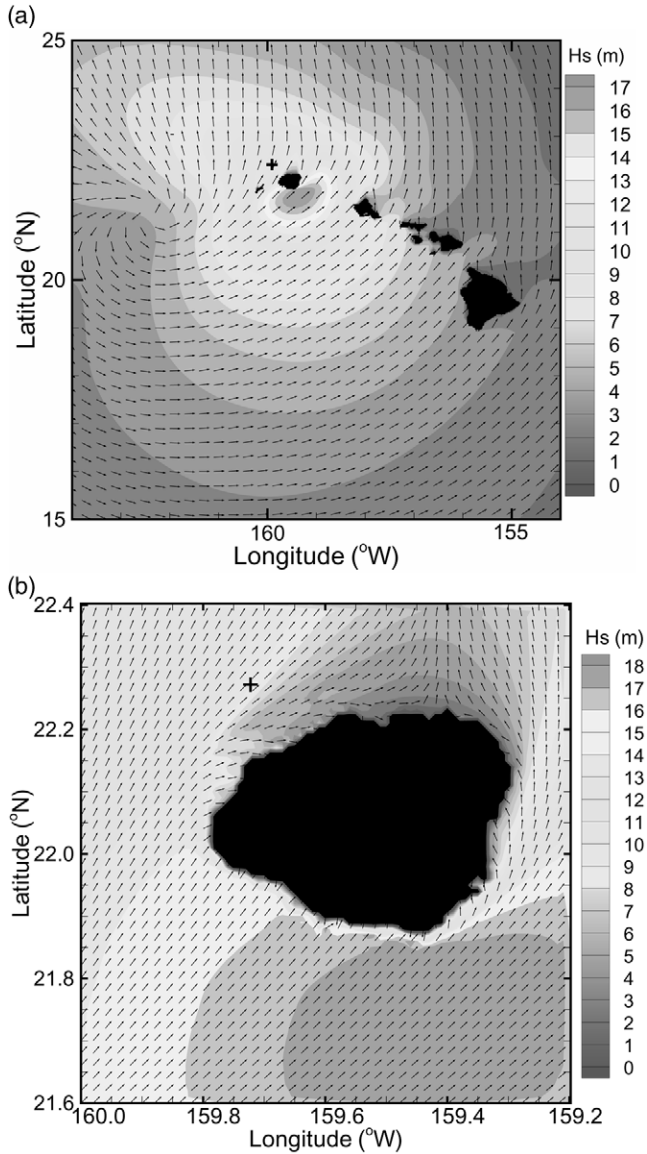


Fig. 12. Wave fields of Hurricane Iwa at closest approach to Kauai. (a) Ocean region. (b) Coastal region. +, storm center.

storm moves past Kauai, the computed significant wave height off the south coast of Oahu reaches 5.5 m. No instruments were operating to measure the offshore wind and wave conditions at the time of the storm and therefore the input wind field and the computed wave heights cannot be verified. Although the wind speeds during Iwa were significantly lower than those during Iniki, the increased fetch from the much larger Iwa results in larger waves than those observed and simulated for Iniki. This agrees with Chiu et al. (1995), who suggested that the storm waves generated by Iwa were larger than those from Iniki based on the extent of underwater damage caused by storm waves around Oahu and Kauai.

More resolved coastal wave fields and estimates of wave setup are needed respectively for the coastal processes simulation in the nearshore region and the storm-water level calculation along the coastline. Figs. 13a and 13b show the wave field and setup in the nested coastal grid off Poipu at the closest approach of Hurricane

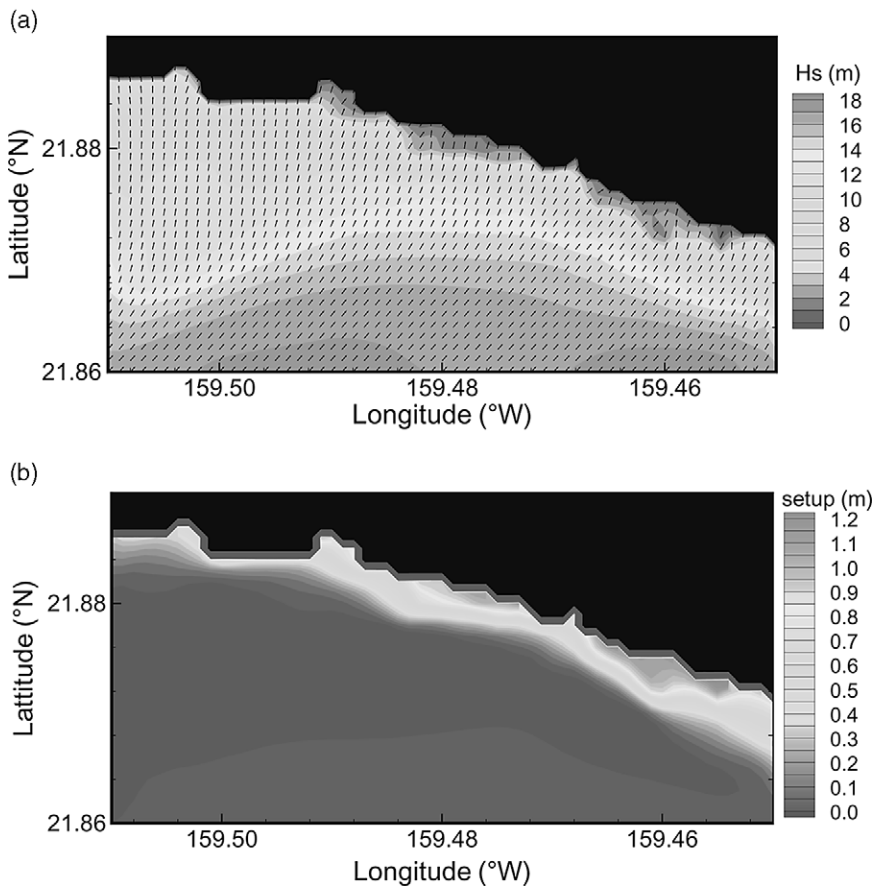


Fig. 13. Wave field and setup in the nested coastal region at Poipu during Hurricane Iwa at closest approach to Kauai. (a) Wave field. (b) Wave setup.

Iwa. The waves approach the computational domain from the southwest and shoal to a maximum significant wave height of 17.8 m at the offshore boundary. The waves break as they propagate toward the coastline and exhibit significant refraction in the nearshore region. Despite the different wave conditions, the computed wave setup shows a pattern similar to that of Iniki. The larger waves of Iwa, however, result in a more extensive surf zone with more vigorous wave breaking activities and a larger wave setup of 1.2 m.

The storm surge, local tides, and wave setup account for the storm-water level. Fig. 14 compares the computed storm-water level and components with tide-gauge measurements at Nawiliwili Harbor. The contribution from the storm surge is smaller in comparison to Iniki, because Iwa was a weaker system and the location of the gauge was further away from the storm center. The maximum wave setup is less than 0.2 m, which is quite small for the computed offshore wave heights. This is due to the sheltering provided by the narrow river estuary for waves approaching parallel to the coastline as shown in Fig. 12. The measured water level shows an offset from the predicted tides before the arrival of the hurricane. Chiu et al. (1983) reported a similar offset of the water-level data recorded by the same type of tide gauges in Honolulu, while the research gauges operated by the University of Hawaii in the same area did not show such a discrepancy. Other than that, the computed water level matches the measured level reasonably well.

The nearshore wave conditions at Poipu are simulated at the time of the closest approach of Iwa. Fig. 15 shows snapshots of the waves in the nearshore region at 6-s intervals after 8 min of simulation. The waves are larger and approach the coastline at large oblique angles comparing to those of Iniki. This results in completely different wave patterns and processes in the surf-zone. The inundation is less compar-

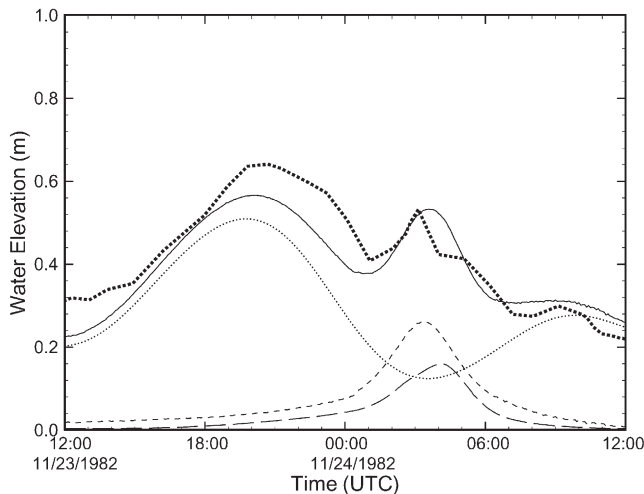


Fig. 14. Comparison of computed and measured water levels during Hurricane Iwa at Nawiliwili Harbor. ·····, astronomical tides; - - - -, storm surge; - · - ·, wave setup; —, storm water elevation; ■, recorded water elevation.

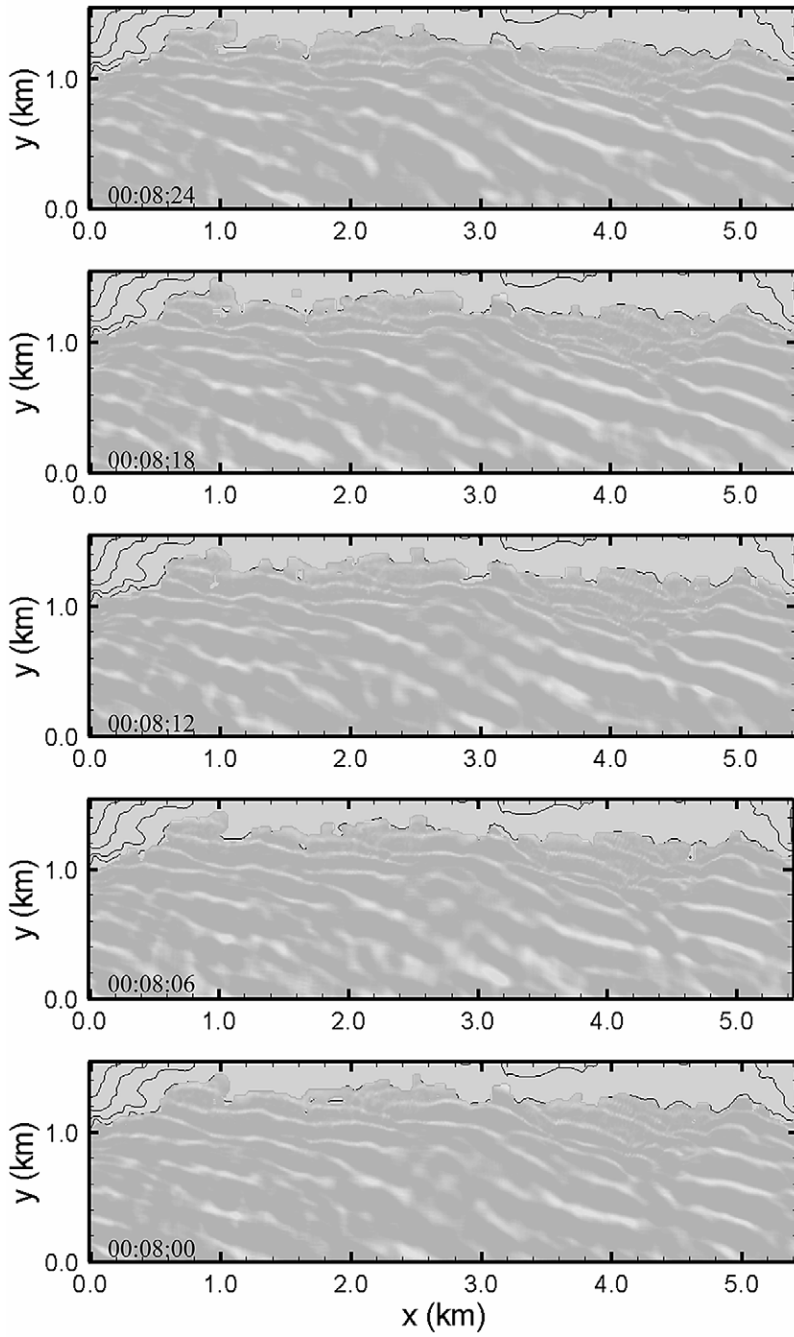


Fig. 15. Wave fields in nearshore region produced by Hurricane Iwa at closest approach to Kauai.

ing to that produced by Iniki, because the waves start breaking and refracting at deeper waters. The momentum of the flow, as indicated by the wave crests, reaches almost to the waterline as opposed to that generated by Iniki. The inundation limit is calculated from a 10-minute simulation. Fig. 16 shows reasonable agreement between the computed inundation limit and the measured debris line, except in the area east of Kukuiula Bay, where the debris line indicates unusually low runup of around 3 m. For the limited storm-water level, the floodwater typically reaches between the 4 and 6-m contours, with a maximum of 8 m near Koloa Landing, once again showing the importance of wave swashing in the inundation.

## **6. Conclusions**

A comprehensive model package has been developed to predict coastal flooding due to tropical cyclone events. The package is composed of four coupled models implemented at three levels of geographic regions to provide simulation of storm wave and surge generation, coastal wave transformation, surf zone processes, and runup onto dry land. The four models are driven by a preprocessor, which generates the computational grids and input atmospheric conditions, manages the data transfer between component models, and automates the simulation process with minimal user intervention. Through the use of a single comprehensive input file, the operation of the package is relatively simple and can easily be adapted to specific user and site requirements. The package adopts a modular structure to allow for easy upgrade and maintenance of the individual components.

Earlier studies have validated the computed wind and wave conditions in the open ocean with buoy and aircraft measurements. The present study focuses on the storm-water levels and inundation produced by Hurricanes Iwa and Iniki, which hit the Hawaiian Island of Kauai in 1982 and 1992 respectively. The two hurricanes had different characteristics and approach directions resulting in different wave and surge conditions. The model results show good agreement with the recorded storm-water levels and overwash debris lines on the south coast of Kauai for both events. The analyses indicate that wave setup can be a significant component of the storm-water level, while wave swashing must be included in the evaluation of the inundation. The present and the earlier studies have demonstrated the capability of the model package as a forecast tool for emergency management and planning in the Pacific insular environment.

## **Acknowledgements**

This work is funded by National Aeronautics and Space Administration, Office of Earth Science, Grant No. NAG5-8748, in collaboration with the Pacific Disaster Center, Hawaii. The authors are thankful to the NWS, WAM, and SWAN communities for their assistance with this project. SOEST Contribution No. 6035.

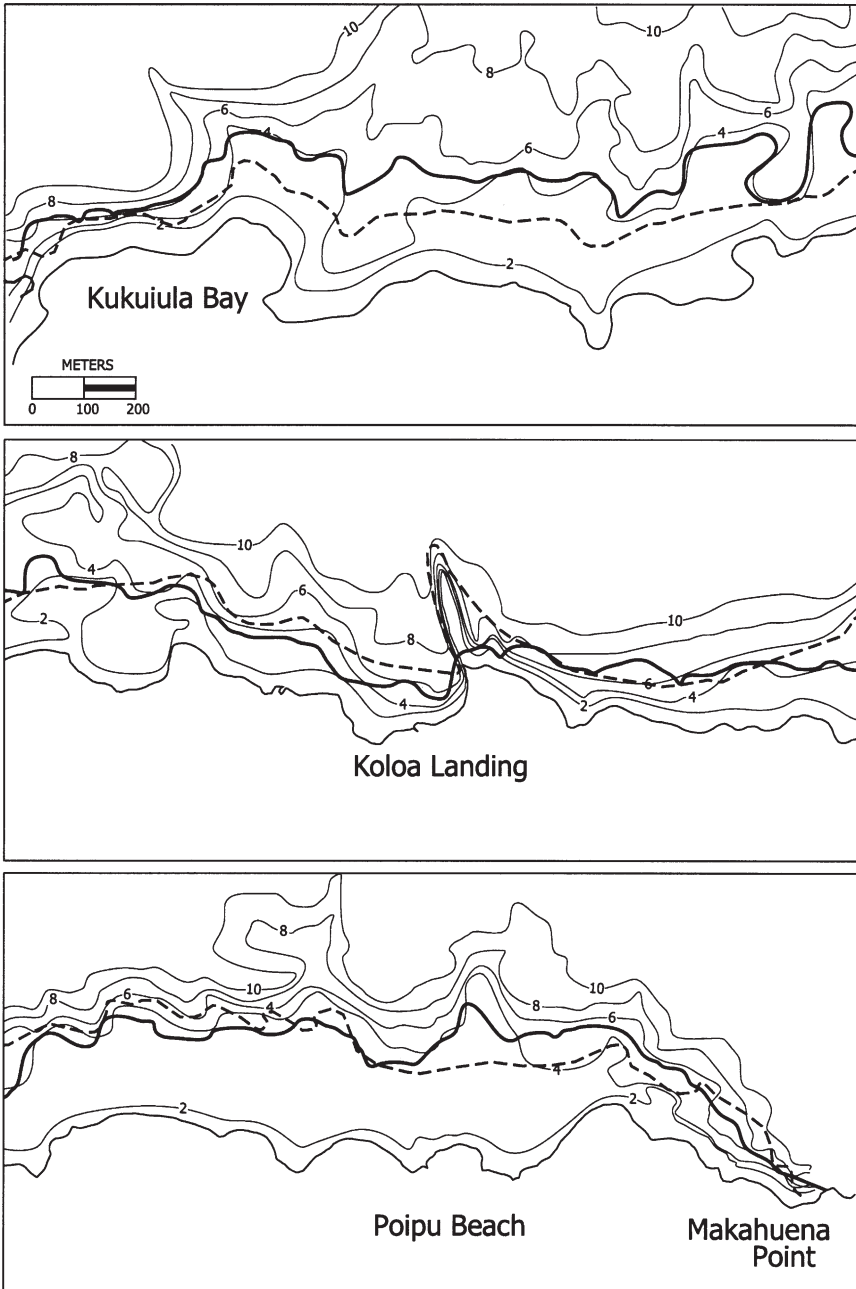


Fig. 16. Comparison of computed and measured inundation at Poipu, Kauai for Hurricane Iwa 1982. -----, overwash debris line; —, computed inundation limit.

## References

- Bao, J.W., Wilczak, J.M., Choi, J.K., Kantha, L.H., 2000. Numerical simulation of air-sea interaction under high wind conditions using a coupled model: A study of hurricane development. *Monthly Weather Review* 128 (7), 2190–2210.
- Bode, L., Hardy, T.A., 1997. Progress and recent development in storm surge modeling. *Journal of Hydraulic Engineering*, ASCE 123 (4), 315–331.
- Booij, N.C., Ris, R.C., Holthuijsen, L.H., 1999. A third-generation wave model for coastal regions. Part I, Model description and validation. *Journal of Geophysical Research* 104 (C4), 7649–7666.
- Bretschneider, C.L., Krock, H.J., Nakazaki, E., Casciano, F.M. 1986. Roughness of Typical Hawaiian Terrain for Tsunami Runup Calculations: A User's Manual. J.K.K. Look Laboratory Report, University of Hawaii, Honolulu, Hawaii.
- Chen, Q., Kirby, J.T., Dalrymple, R.A., Kennedy, A.B., Chawla, A., 2000. Boussinesq modeling of wave transformation, breaking and runup, Part II: Two-dimensional. *Journal of Waterway, Port, Coastal and Ocean Engineering* 126 (1), 48–57.
- Chiu, A.N.L., Escalante, L.E., Mitchell, J.K., Perry, D.C., Schroeder, T.A., Walton, T. 1983. Hurricane Iwa, Hawaii, November 23, 1982. National Academy Press, Washington, D.C.
- Chiu, A.N.L., Chiu, G.L.F., Fletcher, C.H., Krock, H.J., Mitchell, J.K., Schroeder, T.A. 1995. Hurricane Iniki's Impact on Kauai. National Technical Information Service, Springfield, Virginia.
- Chu, P.S., Clark, J.D., 1999. Decadal variations of tropical cyclone activity over the Central North Pacific. *Bulletin of the American Meteorological Society* 80 (9), 1875–1881.
- Douyere, Y.J.-M., 2003. Numerical Modeling of Harbor Oscillation due to Infragravity Waves. M.S. Thesis, Department of Ocean and Resources Engineering, University of Hawaii, Honolulu, Hawaii.
- Flather, R.A., 2000. Existing operational oceanography. *Coastal Engineering* 41 (1-3), 13–40.
- Fletcher, C.H., Richmond, B.M., Barnes, G.M., Schroeder, T.A., 1995. Marine Flooding on the coast of Kauai during Hurricane Iniki: Hindcasting inundation components and delineating washover. *Journal of Coastal Research* 11 (1), 188–204.
- Grell, G.A., Dudhia, J., and Stauffer, D.R., 1994. A Description of the Fifth-Generation Penn State/NCA Mesoscale Model (MM5). Report No. NCAR/TN-398+IA, National Center for Atmospheric Research, Boulder, Colorado.
- Günther, H., Hasselmann, S., and Janssen, P.A.E.M., 1992., The WAM Model Cycle 4. Technical Report No. 4, Deutsches Klimarechenzentrum, Hamburg, Germany.
- Haraguchi, P. 1983. Hurricane Iwa: November 23, 1982. Circular C91, Department of Land and Natural Resources, State of Hawaii, Honolulu, Hawaii.
- Hasselmann, K., Barnett, T.P., Bouws, E., Carlson, H., Cartwright, D.E., Enke, K., Ewing, J.A., Gienapp, H., Hasselmann, E.E., Kruseman, P., Meerburg, A., Mueller, P., Olbers, D.J., Richter, K., Sell, W., Walden, H., 1973. Measurements of wind-wave growth and swell decay during the Joint North Sea Wave Project (JONSWAP). *Deutschen Hydrographischen Zeitschrift* 12 (A8), 7–79.
- Holland, G.J., 1980. An analytic model of the wind and pressure profiles in hurricanes. *Monthly Weather Review* 108 (8), 1212–1218.
- Holthuijsen, L.H., Booij, N., Ris, R.C., Haagsma, I.J.G., Kieftenburg, A.T.M.M., Kriezi, E.E. 2000. SWAN Cycle III Version 40.11 User Manual. Delft University of Technology, The Netherlands.
- Houston, S.H., Shaffer, W.A., Powell, M.D., Chen, J., 1999. Comparison of HRD and SLOSH surface wind fields in hurricanes: Implications for storm surge modeling. *Weather and Forecasting* 14 (5), 671–686.
- Hughes, L.A., 1952. On the low level wind structure of tropical cyclones. *Journal of meteorology* 9, 422–428.
- Janssen, P.A.E.M., 1991. Quasi-linear theory of wind-wave generation applied to wave forecasting. *Journal of Physical Oceanography* 21 (11), 1631–1642.
- Jelesnianski, C.P., 1966. Numerical computations of storm surges without bottom stress. *Monthly Weather Review* 94 (6), 379–394.
- Jelesnianski, C.P., Chen, J., Shaffer, W.A., 1992. SLOSH: Sea, Lake, and Overland Surges from Hurricanes. NOAA Technical Report, NWS 48, Silver Springs, Maryland.

- Kantha, L.H., Clayson, C.A., 1994. An improved mixed layer model for geophysical application. *Journal Geophysical Research* 99 (C12), 25235–25266.
- Kennedy, A.B., Chen, Q., Kirby, J.T., Dalrymple, R.A., 2000. Boussinesq modeling of wave transformation, breaking and runup, Part I: One-dimensional. *Journal of Waterway, Port, Coastal and Ocean Engineering* 126 (1), 39–47.
- Komen, G.J., Cavaleri, L., Donelan, M., Hasselmann, K., Hasselmann, S., Janssen, P.A.E.M., 1994. *Dynamics and Modeling of Ocean Waves*. Cambridge University Press, Cambridge.
- Kowalik, Z., Bang, I., 1987. Numerical computation of tsunami runup by the upstream derivative method. *Science of Tsunami Hazards* 5 (2), 77–84.
- Kurihara, Y., Bender, M.A., Tuleya, R.E., Ross, R.J., 1995. Improvements in the GFDL hurricane prediction system. *Monthly Weather Review* 123 (9), 2791–2801.
- Kurihara, Y., Tuleya, R.E., Bender, M.A., 1998. The GFDL hurricane prediction system and its performance in the 1995 hurricane season. *Monthly Weather Review* 126 (5), 1306–1322.
- Li, Y.S., Zhang, M.Y., 1997. Dynamic coupling of wave and surge models by Eulerian-Lagrangian method. *Journal of Waterway, Port, Coastal & Ocean Engineering, ASCE* 123 (1), 1–7.
- Liu, P.L.-F., Cho, Y.-S., Briggs, M.J., Kanoglu, U., Synolakis, C.E., 1995. Runup of solitary waves on a circular island. *Journal of Fluid Mechanics* 302, 259–285.
- Lynett, P.J., Wu, T.R., Liu, P.L.-F., 2002. Modeling wave runup with depth-integrated equations. *Coastal Engineering* 46 (2), 89–108.
- Martino, C.D., 2000. *Modeling of Hurricane Waves in Hawaiian Waters*. M.S. Thesis, Department of Ocean and Resources Engineering, University of Hawaii, Honolulu, Hawaii.
- Mastenbroek, C., Burgers, G., Janssen, P.A.E.M., 1993. The dynamical coupling of a wave model and a storm surge model through the atmospheric boundary layer. *Journal of Physical Oceanography* 23 (8), 1271–1285.
- Nwogu, O., 1993. Alternative form of Boussinesq equations for nearshore wave propagation. *Journal of Waterway, Port, Coastal, and Ocean Engineering, ASCE* 119 (6), 618–638.
- Ozer, J., Palilla-Hernandez, R., Monbaliu, J., Fanjul, E.A., Albiach, J.C.C., Osuna, P., Yu, J.C.S., Wolf, J., 2000. A coupling module for tides, surges and waves. *Coastal Engineering* 41 (1-3), 95–124.
- Phadke, A.C., Martino, C.D., Cheung, K.F., Houston, S.H., 2003. Modeling of tropical cyclone winds and waves for emergency management. *Ocean Engineering* 30 (4), 553–578.
- Powell, M.D., Houston, S.H., Amat, L.R., Morisseau-Leroy, N., 1998. The HRD real-time hurricane wind analysis system. *Journal of Wind Engineering and Industrial Aerodynamics* 77-78 (1), 53–64.
- Powell, M.D., Houston, S.H., Reinhold, T.A., 1996. Hurricane Andrew's landfall in south Florida. Part I: Standardizing measurements for documentation of surface wind fields. *Weather and Forecasting* 11 (3), 304–328.
- Riegel, B. and Vandamme, R. 2002. *Modeling of Hurricane Winds and Waves: A Case Study of Bonnie 1998*. Projet de Fin d'Études, École navale, Brest, France.
- Ris, R.C., Holthuijsen, H., Booij, N., 1999. A third-generation wave model for coastal regions, Part II, Verification. *Journal of Geophysical Research* 104 (C4), 7667–7681.
- Rogers, W.E., Kaihatu, J.M., Petit, H.A.H., Booij, N., Holthuijsen, L.H., 2002. Diffusion reduction in an arbitrary scale third generation wind wave model. *Ocean Engineering* 29 (11), 1357–1390.
- Rojas, R., 2001. *Development of a Comprehensive Storm Wave Inundation Model*. M.S. Thesis, Department of Ocean and Resources Engineering, University of Hawaii, Honolulu, Hawaii.
- Sea Engineering, Inc., 1993. *Hurricane Iniki — Coastal Inundation Modeling*. Report prepared for the U.S. Army Corps of Engineers, Pacific Ocean Division, Honolulu, Hawaii.
- Sea Engineering, Inc. 2002. *Validation of a Model Package for Storm-Induced Coastal Flooding*. Report prepared for the University of Hawaii, Honolulu, Hawaii.
- Sea Engineering, Inc. and Bretschneider, C.L., 1986. *Hurricane Vulnerability Study for Kauai-Poipu and Vicinity*. Report prepared for the U.S. Army Corps of Engineers, Pacific Ocean Division, Honolulu, Hawaii.
- Skotner, C., Apelt, C.J., 1999a. Application of a Boussinesq model for the computation of breaking waves, Part 1: Development and verification. *Ocean Engineering* 26 (10), 905–925.
- Skotner, C., Apelt, C.J., 1999b. Application of a Boussinesq model for the computation of breaking waves,

- Part 2: Wave-induced setdown and setup on a submerged coral reef. *Ocean Engineering* 26 (10), 927–947.
- Smith, W.H.F., Sandwell, D.T., 1997. Global sea floor topography from satellite altimetry and ship depth soundings. *Science Magazine* 227 (5334), 1956–1962.
- Storm Data, 1992. Outstanding Storms of the Month. NOAA National Climatological Data Center, Asheville, North Carolina.
- Tolman, H.L., 2002. Alleviating the garden sprinkler effect in wind wave models. *Ocean Modelling* 4 (3–4), 269–289.
- Tolman, H.L., Balasubramaniyan, B., Burroughs, L.D., Chalikov, D.V., Chao, Y.Y., Chen, H.S., Gerald, V.M., 2002. Development and implementation of wind generated ocean surface wave models at NCEP. *Weather and Forecasting* 17 (2), 311–333.
- WAMDI Group., 1988. The WAM model — a third generation ocean wave prediction model. *Journal of Geophysical Research*, 18(12), 1775–1810.
- Wei, G., Kirby, J.T., Sinha, A., 1999. Generation of waves in Boussinesq models using a source function method. *Coastal Engineering* 36 (4), 271–299.
- Wessel, P., Smith, W.H.F., 1991. Free software helps map and display data. *EOS Transactions of American Geophysics Union* 72 (41), 441–446.
- Westerink, J.J., Luettich, R.A., Baptista, A.M., Scheffner, N.W., Farrar, P., 1992. Tide and storm surge predictions using finite element model. *Journal of Hydraulic Engineering, ASCE* 118 (10), 1373–1390.
- Wong, G.T., 2003. Calibration of a Boussinesq Coastal Processes and Runup Model: A Case Study of Waimea Bay, Hawaii. M.S. Thesis, Department of Ocean and Resources Engineering, University of Hawaii, Honolulu, Hawaii, in preparation.
- Wornom, S.F., Welsh, D.J.S., Bedford, K.W., 2001. On coupling of the SWAN and WAM wave models for accurate nearshore wave predictions. *Coastal Engineering Journal* 43 (3), 161–201.
- Wright, C.W., Walsh, E.J., Vandemark, D., Krabill, W.B., Houston, S.H., Powell, M.D., Black, P.G., Marks, F.D., 2001. Hurricane directional wave spectrum spatial variation in the open ocean. *Journal of Physical Oceanography* 31 (8), 2472–2488.
- Zambresky, L. 1989. A Verification Study of the Global WAM Model December 1987– November 1988. Report No. 63, European Center for Medium Range Weather Forecasts, Reading, England.
- Zelt, J.A., 1991. The runup of nonbreaking and breaking solitary waves. *Coastal Engineering* 15 (3), 205–246.